The Inhibition Mechanism of Emodin to the Core Protein of Aeromonas Hydrophila at the Molecular Level

Huimin Zhang (18114862671@163.com)
Nanjing Agricultural University
Bo Liu
Nanjing Agricultural University
Xianping Ge
Nanjing Agricultural University

Research Article

Keywords: Aeromonas hydrophila, Emodin, atpE, Inhibition mechanism, Molecular dynamics simulation

Posted Date: June 14th, 2021

DOI: https://doi.org/10.21203/rs.3.rs-452162/v1

Abstract

Aeromonas hydrophila is a main pathogen and is of great harm in aquaculture, but the effective methods to inhibit it is not clear. This study reveals that emodin inhibits the activity of *A. hydrophila* through experimental methods. Further proteomics analysis showed that atpE was the core protein of the inhibition. To disclose how emodin affects the inhibition mechanism, molecular docking and molecular dynamics simulations were carried out for *A. hydrophila* core protein binding with emodin. Comparing with these simulations of free atpE, this study uncovered that the inhibition of emodin involves emodin directly binding to core protein atpE with this simulations. The emodin engages with residues TYR10, ALA13, ALA14, MET17, LEU70 and TYR73 of atpE, which eventually leads to the inhibition of the activity of *A. hydrophila*. Additionally, this phenomenon was confirmed by the experimental results. The finding provides a novel insight for the study of the underlying mechanisms of emodin on antimicrobial activity of *A. hydrophila* at the molecular level.

1. Introduction

Aeromonas hydrophila widely exists in water and soil [1]. It can not only cause the outbreak of motile aeromonad septicemia in aquatic animals, resulting in a large number of deaths, but also cause human gastroenteritis and hemorrhagic disease, threatening human health. Previous researches report that *A. hydrophila* can induce sepsis, a serious disease in the fish farming industry, which has caused severe economic losses to fisheries [2, 3, 4, 5, 6]. Many factors such as cytotoxins, adhesins, and hemolysins as well as metabolic pathways, biofilms formation specific, and virulence factor expression regulation have been confirmed to be related to the virulence of *A. hydrophila* [7, 8, 9]. However, the inhibition mechanism of *A. hydrophila* at molecular level is still uncertain, it is an urgent need to probe the underlying mechanism to restrain pathogens.

Emodin (1, 3, 8-trihydroxy-6-methyl-anthraquinone) is a kind of monomer (Fig. 1) isolated from rhubarb, Polygonum cuspidatum, Polygonum multiflorum and other plants [10, 11]. To date, emodin has growth-inhibitory and cytotoxic effects on a variety of bacteria such as *A. hydrophila* [12, 13]. At the same time, many studies have shown that emodin as a feed additive can enhance the immunity of fish to *A. hydrophila* infection [14, 15]. However, most of the current research focuses on the changes in physical structures and bacteriostatic concentration, and lack of research on key targets. Therefore, it is important to understand the exact molecular mechanism by which emodin inhibits *A. hydrophila* and find effective targets for emodin.

In recent years, computer-assisted drug design methods have developed rapidly, and these methods have achieved high accuracy that allows them to be routinely applied in the in-depth interpretation of experiments and drug discovery campaigns [16, 17]. Protein structure-based methods are useful for predicting the binding modes of small molecules and their relative affinities. High-throughput molecular docking of up to 10^6 small molecules and scoring based on implicit solvent force fields can reliably identify micro-polar binding partners using rigid protein targets. Explicit solvent molecular dynamics (MD)

simulation is a low-throughput technique used to characterize flexible binding sites and accurately evaluate binding pathways, kinetics, and thermodynamics. This method can be used to guide experiments and explain experimental phenomena [17, 18, 19, 20]. MD simulations have long been thought to provide insights into protein dynamics, not just insights into available crystal structures, and reveal new cryptic binding sites, extending the drug properties of targets. One of the first methods described is the relaxation complex scheme, which combines all-atomic nanosecond-long molecular dynamics simulations of protein targets to describe its conformational flexibility, while small molecules quickly dock to proteins stored in molecular dynamics snapshot [21, 22]. This method has been successfully applied to a variety of cancer-related MDM2/MDMx-p53 interactions [23] or HIV integrase [24]. It is gratifying that in the latter case, the hidden pocket first proposed *in silico* has been experimentally validated and approved for the development of clinical enzyme inhibitors against HIV infection [25].

Therefore, we performed molecular docking and MD simulations to assess the inhibition mechanism of *A. hydrophila* under the influence of emodin on the basis of the experiments. The mode of binding of emodin to *A. hydrophila* core protein and interaction with residues was analyzed combing with experimental data. This study provides the underlying mechanism of inhibition behavior of the core protein of *A. hydrophila* under emodin at the molecular level.

2. Methods

2.1 Culture of A. hydrophila

A. hydrophila (NJ-35) was obtained from cyprinid in Jiangsu Province, China [26], and offered by Professor Yong-jie Liu from Nanjing Agricultural University, P.R. China. Emodin was purchased from Kono Chem Co., Ltd, Xi'an, China. This emodin has a purity of 98%. Six concentrations of emodin (0, 100, 200, 300, 400, and 500 μm/ml) in normal Luria Broth medium (LB; BD; final pH = 7.4) were selected to measure the amount of *A. hydrophila* NJ-35.

2.2 RT-PCR analysis ad RNA extraction

The total RNA of *A. hydrophila* NJ-35 from the two groups (9 samples per group) were extracted by RNAiso Plus (TaKaRa, Japan) and tested by Nanodrop 2000 (Thermo Fisher Scientific, USA). The RNA in each sample was diluted to 10 ng/ml. After that the quantitative analysis were performed on 2 μg of the total RNA using the Two Steps SYBR® PrimeScript® Plus RT-PCR Kit (TaKaRa, Dalian). Based on the method of Liu et al. [27], the Real-time quantitative PCR (RT-PCR) was adopted. ABI 7500 real-time PCR system was conducted for detection and the $2^{-\triangle\triangle CT}$ technique was used for further analysis.

2.3 Molecular docking calculations

The docking simulations were implemented by the molecular docking algorithm [28]. The atomic structures of emodin for the docking calculations were obtained from the protein data bank (http://www.rcsb.org/). Meanwhile, the homology model of atpE was obtained through the SWISS MODEL (https://swissmodel.expasy.org/). The potential CHRMM36 force fields were adopted, which was accurately adopt in different simulations based on experimental results [29].

2.4 Molecular Dynamics Simulations

MD simulations were performed with the GROMACS 5.1.3 through the potential of GROMOS96 54a7 force field [30]. The lowest binding energy (the most negative) docking conformation generated by the software Autodock was taken as the initial conformation of MD simulation. The topological structure parameters of proteins were established by GROMACS program. The topological parameters of emodin were generated by Dundee PRODRG server. The simulation models were immersed in a tetrahedral box full of water. The solvation system (emodin, atpE and water) was neutralized by adding 2 Na ions. In order to release the collision contact, 50000 steps steepest descent method and 50000 steps conjugate gradient calculations were used to minimize the energy. MD simulation study includes equilibration stage and production stage. In order to balance the system, a 500 ps position constrained kinetic simulation (NVT and NPT) of solute (protein, anti-ion and emodin) was carried out at 300 K. Finally, the MD production of 100000 ps was carried out at 300 K and 1 bar pressure. The software of VMD is used for visualization [31].

2.5 MM/PBSA calculations

The binding free energies of atpE-emodin complex were obtained by the Molecular Mechanics Generalized Born Surface Area (MM/PBSA) methodology [32, 33] based on

$$\Delta G_{binding} = \Delta E_{MM} + \Delta G_{sol} - T\Delta S,$$

where, ΔE_{MM} is the energy of molecular mechanics interactions, including van der Waals energy and electrostatic energy. Where ΔG_{sol} is the solvation free energy calculated via continuum solvent methods, which can be divided into nonpolar ($\Delta G_{nonpolar}$) and electrostatic (ΔG_{polar}) contributions. The nonpolar component ($\Delta G_{nonpolar}$) was expressed as $\Delta G_{nonpolar} = \lambda \mathrm{SASA} + b$, where, b = 0.92 kcal mol^{-1} and λ = 0.00542 kcal $Å^{-2}$[34], this component is a function of solvent accessible surface area (SASA). ΔG_{polar} is calculated through solving the Poisson-Boltzmann equations. Where $-T\Delta S$ is the entropy change, which was ignored here due to the low prediction accuracy and large computational overhead [35, 36]. The entropy term also was ignored. Thus, the free energy obtained is not true binding energy. Besides, a per-residue decomposition of the total energy by the MM/GBSA algorithm was also carried out to assess the contribution of each residue to the binding. The polarity contribution of desolvation was calculated by GB model [37]. A more detailed theory of energy decomposition is described elsewhere [38].

3. Results And Discussions

3.1 Emodin inhibits the activity of *A. hydrophila*

As shown in Fig. 2, with the increasing of the emodin concentration, the concentration of *A. hydrophila* decreased in a dose-dependent manner. The OD600 under the concentrations of 0 and 100 were almost the same. However, the concentrations of 200, 300, 400, and 500 μm/ml emodin groups were significantly different from the control group, and there were also significant differences between them, indicating that emodin can inhibit the growth of *A. hydrophila*. According to Fig. 2, the relative expression of atpE was at high level, but the expression was significantly down-regulated under the action of emodin, which indicates that atpE is a target site of emodin binding.

3.2 The binding mechanism of atpE with emodin

Computer-aided drug design was further performed to characterize the detailed mechanisms of this inhibition. Yet, many researches have shown that atpE at the protein was down-regulated under emodin treatment, the molecular mechanisms of inhibition expression remain elusive. Here, we hope to determine the potential binding of emodin to atpE by molecular docking and MD simulation. In order to study the mechanism of emodin inhibiting atpE, the preferred binding mode of atpE and emodin was determined by 10 ns MD simulation based on the docking results of emodin with atpE. In this calculations, emodin represents a kind of ligand, which binds to atpE through molecular mechanical interaction. During the simulation, emodin was localized to the region of atpE. VMD software was used to predict the binding mode of emodin with atpE and the binding energy of each residue [31] as illustrated in Fig. 3a. Figure. 3b showed that the key residues around emodin. Specially, the binding models (Fig. 3b) revealed that the TYR10, ALA13, ALA14, MET17, TYR73 and LEU70 anchor emodin. As shown in Fig. 3b, the chains of TYR10 and LEU70 were close to the emodin, indicating that TYR10 and LEU70 have strong interactions with emodin. Moreover, Fig. 3b shows that the benzene ring plane of emodin in atpE complex is parallel to that of residue. TYR10 and TYR10 were also close to emodin. Therefore, a strong interaction between emodin and these residues exists. These calculations will be further proved by the analysis of energy decomposition.

The root meant square fluctuation (RMSF) of all residues of free atpE and atpE-emodin complex (residues 1–79) was shown to uncover the flexibility of all the residues. As shown in Fig. 4, the RMSF of these residues clearly depicted the different flexibility of atpE binding sites in the complex. In the case of RMSF less than 0.60 nm in the complex, all residues in the atpE binding sites (residues 10–20 and 60–75) of emodin exhibited small degree of flexibility, showing that these residues became more rigid due to their binding to emodin. The regions are colored with yellow that binds with emodin show small degree of flexibility with low RMSF (less than 0.6 nm) when compared with free atpE. This indicates that these residues seem to be more rigid because of binding to atpE. Figure. 3b shows that the stability of atpE binding cavity in the complex was mainly due to residues TYR10, ALA13, ALA14, MET17, LEU70 and TYR73.

The root-mean-square deviation (RMSD) of the backbone atoms with regard to the initial confirmation was obtained as a function of simulation time. The value of RMSD is to evaluate the conformational

stability of the complex during the simulations. Figure. 5a showed that the mean value of RMSD profile of the free atpE is 0.32 nm, which is higher than complex of 0.29 nm for the simulation process. The result showed that the conformation of the MD simulations after energy minimization was reliable for analyses. This indicates that the atpE in the complex is very rigid due to the constraint of emodin. On the other hand, Fig. 5b showed that the radius of gyration of complex bound conformation was found less than free atpE, indicating that the complex with the low radius of gyration and more stable.

3.3 The binding site in the atpE-emodin complex

In order to access the energetic effects on the contributions of key residues, the interaction energy between atpE and emodin was modeled based on the energy decomposition of the residues (Fig. 6a). The main energy contributions from − 8 to -1.5 kJ mol^{-1} mainly came from TYR10, ALA13, ALA14, MET17, LEU70 and TYR73. These data agree with the described in Fig. 3 of the MD simulation results. Figure 6b showed that the binding mode of emodin with atpE. In this binding mode, color from red to blue represented total free energy from low to high. The results showed that emodin and atpE had a good binding effect.

In order to obtain underlying mechanism about the residues around the binding sites and their contribution to the complex, the molecular mechanics, polar, nonpolar and total energy contribution of the residues to the binding free energy were calculated by MM/PBSA algorithm. The analysis was performed using 1000 snapshots obtained from the 10 ns simulations. The sum of the each residue free energies were separated into molecular mechanics (ΔE_{MM}), polar (ΔE_{Polar}), nonpolar (ΔE_{APolar}), and total contribution (ΔE_{Total}). The energy decompositions from the key residues were showed in Fig. 7. We can see that the atpE-emodin complex, TYR73 has an appreciable molecular mechanics (ΔE_{MM}) contribution, with a ΔE_{MM} of -12 kJ/mol. In fact, TYR73 was close to the ligand of emodin, and more molecular mechanics interactions exist between atpE and emodin. Besides, residue TYR10, with a ΔE_{MM} of -8.5 kJ/mol, has a strong molecular mechanics interaction with the ligand due to the close proximity between the emodin and residue TYR10, which facilitates a strong pep interaction in the atpE-emodin complex. For all the residues, the major decomposed energy interaction originated from molecular mechanics interactions, the second was by the polar interactions, while nonpolar contribution showed a minor effect on the formation of key residues in atpE-emodin complex. With the summation of the other energy term, an estimated ΔE_{bind} of -0.271 kJ/mol was showed for emodin, indicating that emodin can strongly interact and bind with the binding site of atpE. These simulation results well explain the mechanism of emodin in inhibiting the activity of *A. hydrophila*.

4. Conclusions

In this paper, the growth curves of *A. hydrophila* at 0, 100, 200, 300, 400, and 500 μm/ml emodin were determined, and the gene expression level of atpE was measured. The results showed that emodin has a good inhibition effect of *A. hydrophila*, and atpE was the core protein of the inhibition. In order to understand the effect of emodin on the inhibition mechanism, MD simulations were performed for *A.*

hydrophila core protein blinding with emodin. By this method, the analysis showed that the inhibitory of emodin involves the direct binding of emodin to the core protein atpE. The emodin engages with residues TYR10, ALA13, ALA14, MET17, LEU70 and TYR73 of atpE, which eventually led to inhibition of the activity. This mechanism was verified by the experimental results. The finding provides a novel insight for the study of mechanism of emodin on antimicrobial activity of *A. hydrophila* at molecular level.

Declarations

Competing Financial Interests Statement

The authors declare no competing financial interests.

Acknowledgment

This work was supported by the Central Public-interest Scientific Institution Basal Research Fund, CAFS (2018HY-ZD0501), the National Natural Science Foundation of China (31772867), the Modern Agriculture Industrial Technology System (CARS-48), the Independent Innovation of Agricultural Science and Technology in Jiangsu province (CX(17)2027)and “333 High Level Talent Project” of Jiangsu Province (BRA2018154), and Scientific Research Foundation for the Returned Overseas Chinese Scholars in Wuxi City (201708)). The authors gratefully acknowledge the postgraduate students of the Fish Disease and Nutrition Department, FFRC, CAFS, Wuxi City, PR China for their assistance during the sampling period.

Author Declaration

Availability of data and material: The atomic structures of emodin for the docking calculations were obtained from the protein data bank (http://www.rcsb.org/). Meanwhile, the homology model of atpE was obtained through the SWISS MODEL (https://swissmodel.expasy.org/).

Code availability:

All the software used in this paper are open source software, which can be downloaded on the Internet.

Authors' contributions:

The manuscript was written through contributions of all authors. Huimin Zhang: Methodology, Software, Data curation, Investigation, Visualization, Writing - original draft, Writing - review & editing. Bo Liu: Conceptualization, Supervision, Writing - review & editing. Xianping Ge: Conceptualization, Supervision, Writing - review & editing. All authors have given approval to the final version of the manuscript.

References

1. Kaper J, Lockman H, Colwell R, Joseph S (1981) Aeromonas hydrophila: ecology and toxigenicity of isolates from an estuary. J Appl Bacteriol 50:359–377
2. Stratev D, Odeyemi OA (2016) Antimicrobial resistance of Aeromonas hydrophila isolated from different food sources: A mini-review. J Infect Public Heal 9:535–544
3. Zhang D, Xu D-H, Shoemaker C (2016) Experimental induction of motile Aeromonas septicemia in channel catfish (Ictalurus punctatus) by waterborne challenge with virulent Aeromonas hydrophila. Aquaculture Reports 3:18–23
4. Pang M, Xie X, Dong Y, Du H, Wang N, Lu C, Liu Y (2017) Identification of novel virulence-related genes in Aeromonas hydrophila by screening transposon mutants in a Tetrahymena infection model. Vet Microbiol 199:36–46
5. Abd-El-Rhman AM (2009) Antagonism of Aeromonas hydrophila by propolis and its effect on the performance of Nile tilapia, Oreochromis niloticus. Fish Shellfish Immunol 27:454–459
6. Liu J, Xie L, Zhao D, Yang T, Hu Y, Sun Z, Yu X (2019) A fatal diarrhoea outbreak in farm-raised Deinagkistrodon acutus in China is newly linked to potentially zoonotic Aeromonas hydrophila. Transbound Emerg Dis 66:287–298
7. Rasmussen-Ivey CR, Figueras MJ, McGarey D, Liles MR (2016) Virulence factors of Aeromonas hydrophila: in the wake of reclassification. Front Microbiol 7:1337
8. Qin Y, Lin G, Chen W, Xu X, Yan Q (2016) Flagellar motility is necessary for Aeromonas hydrophila adhesion. Microb Pathogenesis 98:160–166
9. Zhang H, Song C, Xie J, Ge X, Liu B, Zhang Y, Sun C, Zhou Q, Yang Z (2018) Comparative proteomic analysis of hepatic mechanisms of Megalobrama amblycephala infected by Aeromonas hydrophila. Fish Shellfish Immunol 82:339–349
10. Xiao P, He L, Wang L (1984) Ethnopharmacologic study of chinese rhubarb. J Ethnopharmacol 10:275–293
11. Liu Z, Wei F, Chen LJ, Xiong HR, Liu YY, Luo F, Hou W, Xiao H, Yang ZQ (2013) In vitro and in vivo studies of the inhibitory effects of emodin isolated from Polygonum cuspidatum on Coxsakievirus B(4). Molecules 18:11842–11858
12. Duan F, Xin G, Niu H, Huang W (2017) Chlorinated emodin as a natural antibacterial agent against drug-resistant bacteria through dual influence on bacterial cell membranes and DNA. Sci Rep 7:12721
13. Huy TXN, Reyes AWB, Hop HT, Arayan LT, Son VH, Min W, Lee HJ, Kim S (2018) Emodin Successfully Inhibited Invasion of Brucella abortus Via Modulting Adherence, Microtubule Dynamics and ERK Signaling Pathway in RAW 264.7 Cells. J Microbiol Biotechnol 28:1723–1729
14. Harikrishnan R, Jawahar S, Thamizharasan S, Paray BA, Al-Sadoon MK, Balasundaram C (2018) Immune defense of emodin enriched diet in Clarias batrachus against Aeromonas hydrophila. Fish Shellfish Immunol 76:13–20

15. Liu F, Shi HZ, Guo QS, Yu YB, Wang AM, Lv F, Shen WB (2016) Effects of astaxanthin and emodin on the growth, stress resistance and disease resistance of yellow catfish (Pelteobagrus fulvidraco). Fish Shellfish Immunol 51:125–135
16. Śledź P, Caflisch A (2018) Protein structure-based drug design: from docking to molecular dynamics. Curr Opin Struc Biol 48:93–102
17. Ge Y, van der Kamp M, Malaisree M, Liu D, Liu Y, Mulholland AJ (2017) Identification of the quinolinedione inhibitor binding site in Cdc25 phosphatase B through docking and molecular dynamics simulations. J Comput Aid Mol Des 31:995–1007
18. Niu X, Qiu J, Wang X, Gao X, Dong J, Wang J, Li H, Zhang Y, Dai X, Lu C, Deng X (2013) Molecular insight into the inhibition mechanism of cyrtominetin to alpha-hemolysin by molecular dynamics simulation. Eur J Med Chem 62:320–328
19. Ivetac A, McCammon JA (2009) Elucidating the Inhibition Mechanism of HIV-1 Non-Nucleoside Reverse Transcriptase Inhibitors through Multicopy Molecular Dynamics Simulations. J Mol Biol 388:644–658
20. Firdayani FF, Arsianti A, Churiyah CC, Yanuar A (2018) Molecular Docking and Dynamic Simulation Studies of Benzoylated Emodin into HBV Core Protein. Journal of Young Pharmacists 10:S20–S24
21. Lin JH, Perryman AL, Schames JR, McCammon JA. The relaxed complex method: Accommodating receptor flexibility for drug design with an improved scoring scheme. Biopolymers: Original Research on Biomolecules. 2003;68:47–62
22. Amaro RE, Baron R, McCammon JA (2008) An improved relaxed complex scheme for receptor flexibility in computer-aided drug design. J Comput Aid Mol Des 22:693–705
23. Barakat K, Mane J, Friesen D, Tuszynski J (2010) Ensemble-based virtual screening reveals dual-inhibitors for the p53–MDM2/MDMX interactions. J Mol Graph Model 28:555–568
24. Schames JR, Henchman RH, Siegel JS, Sotriffer CA, Ni H, McCammon JA (2004) Discovery of a novel binding trench in HIV integrase. J Med Chem 47:1879–1881
25. Hazuda DJ, Anthony NJ, Gomez RP, Jolly SM, Wai JS, Zhuang L, Fisher TE, Embrey M, Guare JP, Egbertson MS. A naphthyridine carboxamide provides evidence for discordant resistance between mechanistically identical inhibitors of HIV-1 integrase. Proceedings of the National Academy of Sciences. 2004;101:11233-8
26. Pang M, Jiang J, Xie X, Wu Y, Dong Y, Kwok AHY, Zhang W, Yao H, Lu C, Leung FC (2015) Novel insights into the pathogenicity of epidemic Aeromonas hydrophila ST251 clones from comparative genomics. Sci Rep-Uk 5:9833
27. Liu B, Xu L, Ge X, Xie J, Xu P, Zhou Q, Pan L, Zhang Y (2013) Effects of mannan oligosaccharide on the physiological responses, HSP70 gene expression and disease resistance of Allogynogenetic crucian carp (Carassius auratus gibelio) under Aeromonas hydrophila infection. Fish Shellfish Immun 34:1395–1403
28. Pagadala NS, Syed K, Tuszynski J (2017) Software for molecular docking: a review. Biophysical reviews 9:91–102

29. Lee J, Cheng X, Jo S, Mackerell AD, Im W (2016) CHARMM-GUI Input Generator for NAMD, Gromacs, Amber, Openmm, and CHARMM/OpenMM Simulations using the CHARMM36 Additive Force Field. Biophys J 110:641a
30. Schmid N, Eichenberger AP, Choutko A, Riniker S, Winger M, Mark AE, van Gunsteren WF (2011) Definition and testing of the GROMOS force-field versions 54A7 and 54B7. European biophysics journal 40:843
31. Humphrey W, Dalke A, Schulten K (1996) VMD: visual molecular dynamics. J Mol Graph 14:33–38
32. Massova I, Kollman PA (2000) Combined molecular mechanical and continuum solvent approach (MM-PBSA/GBSA) to predict ligand binding. Perspectives in drug discovery design 18:113–135
33. Kollman PA, Massova I, Reyes C, Kuhn B, Huo S, Chong L, Lee M, Lee T, Duan Y, Wang W (2000) Calculating structures and free energies of complex molecules: combining molecular mechanics and continuum models. Accounts Chem Res 33:889–897
34. Sitkoff D, Sharp KA, Honig B (1994) Accurate calculation of hydration free energies using macroscopic solvent models. The Journal of Physical Chemistry 98:1978–1988
35. Wang W, Kollman PA. Computational study of protein specificity: the molecular basis of HIV-1 protease drug resistance. Proceedings of the National Academy of Sciences. 2001;98:14937-42
36. Wang J, Morin P, Wang W, Kollman PA (2001) Use of MM-PBSA in reproducing the binding free energies to HIV-1 RT of TIBO derivatives and predicting the binding mode to HIV-1 RT of efavirenz by docking and MM-PBSA. J Am Chem Soc 123:5221–5230
37. Jayaram B, Sprous D, Beveridge D (1998) Solvation free energy of biomacromolecules: Parameters for a modified generalized Born model consistent with the AMBER force field. J Phys Chem B 102:9571–9576
38. Gohlke H, Kiel C, Case DA (2003) Insights into protein–protein binding by binding free energy calculation and free energy decomposition for the Ras–Raf and Ras–RalGDS complexes. J Mol Biol 330:891–913

Figures

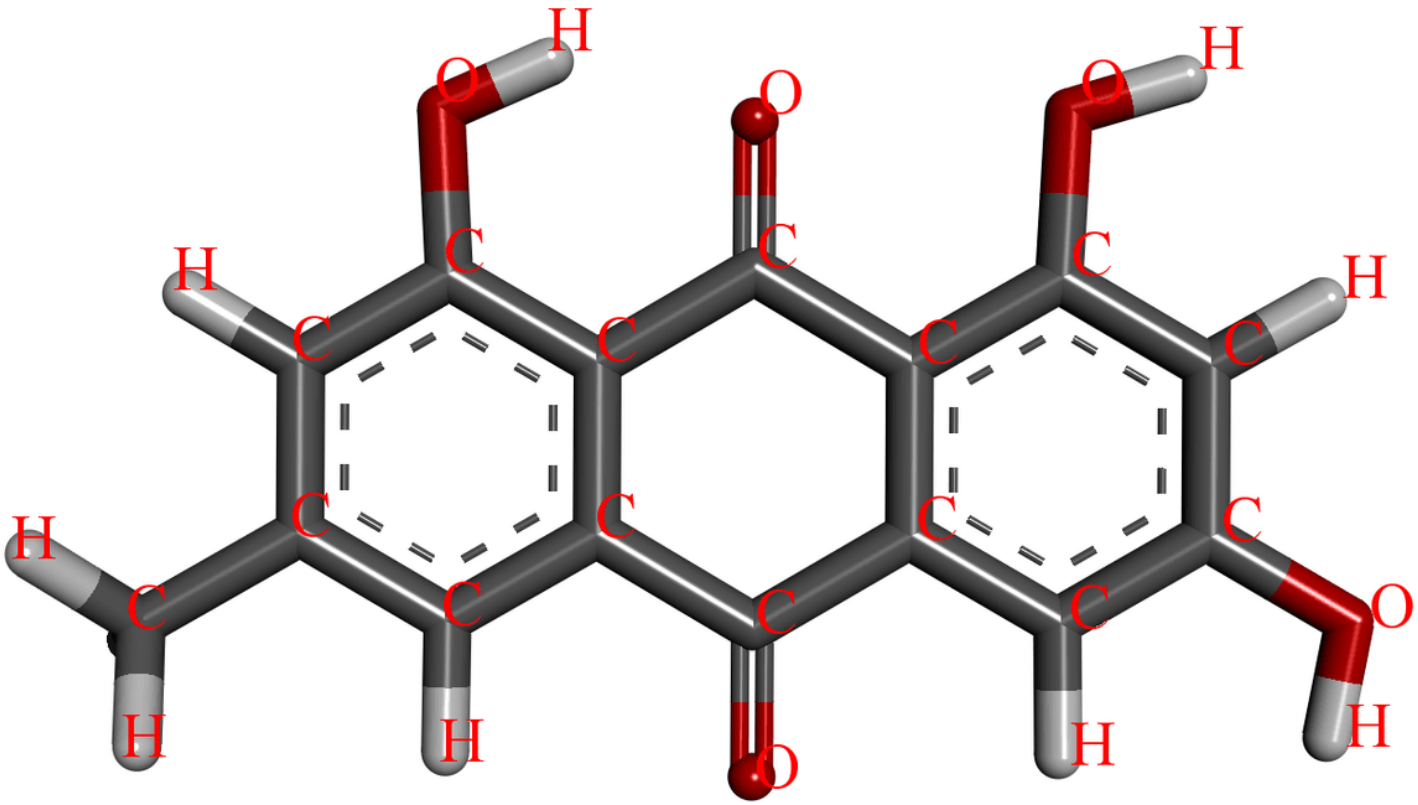

Figure 1

Chemical structure of emodin with the atom and moiety names used in this study

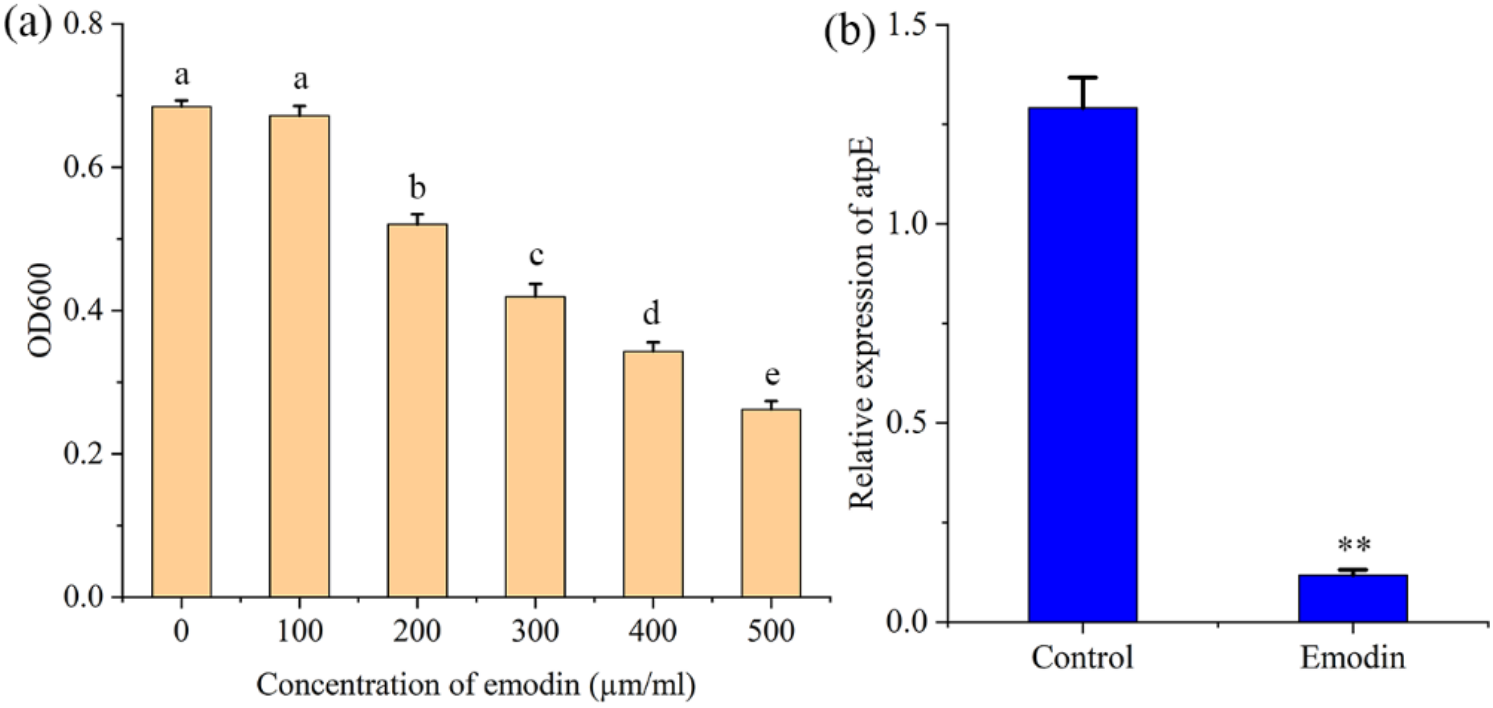

Figure 2

The inhibition of emodin on A. hydrophila. (a) Effect of emodin supplementation on growth A. hydrophila for 12 h. (b) The inhibition of emodin on the atpE by qRT-PCR.

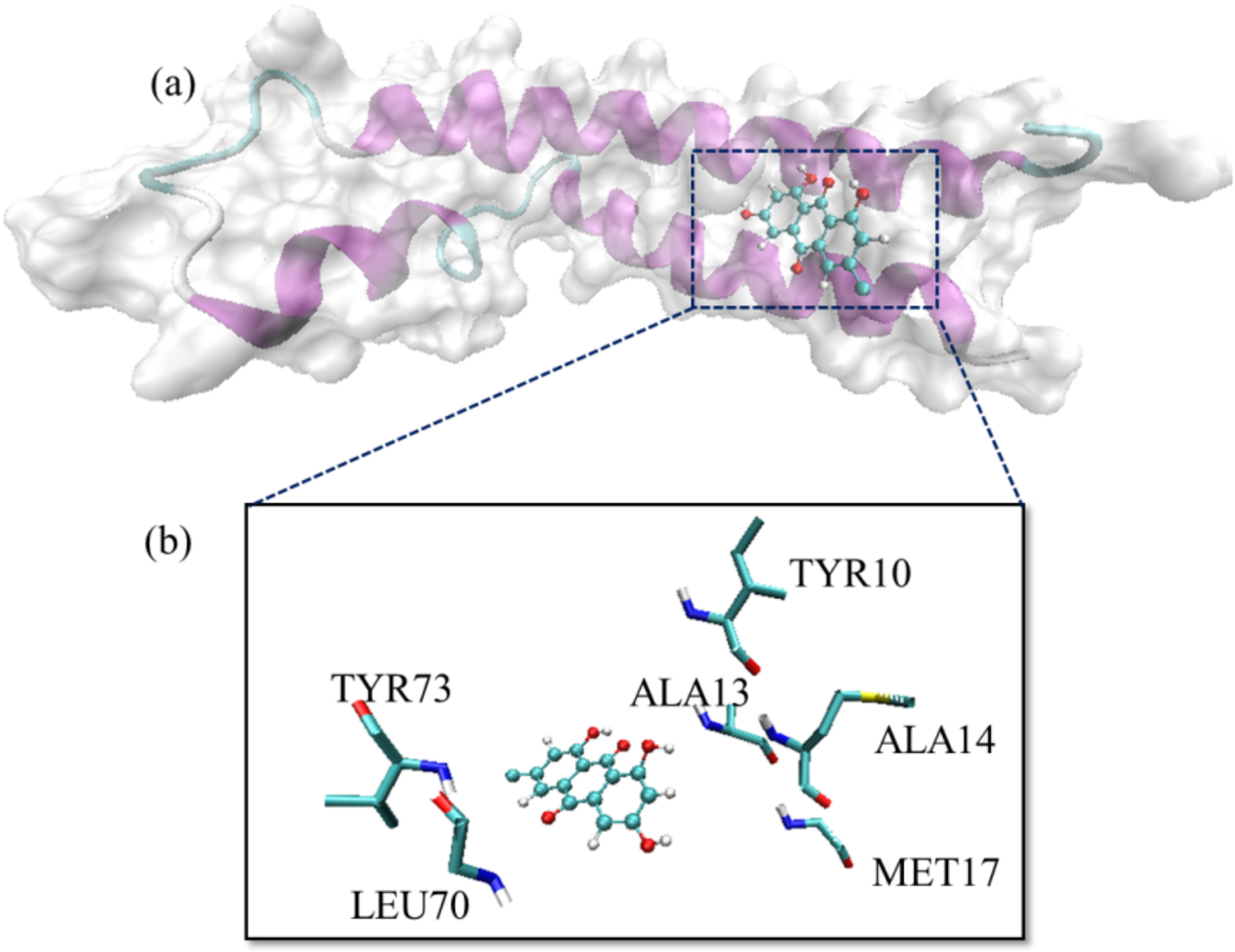

Figure 3

The final structure of the binding modes of emodin with atpE obtained after MD simulation. (a) 3D structure of binding structure of emodin with atpE. (b) The structure of the binding mode showed the interaction of emodin to residues TYR10, ALA13, ALA14, MET17, LEU70 and TYR73.

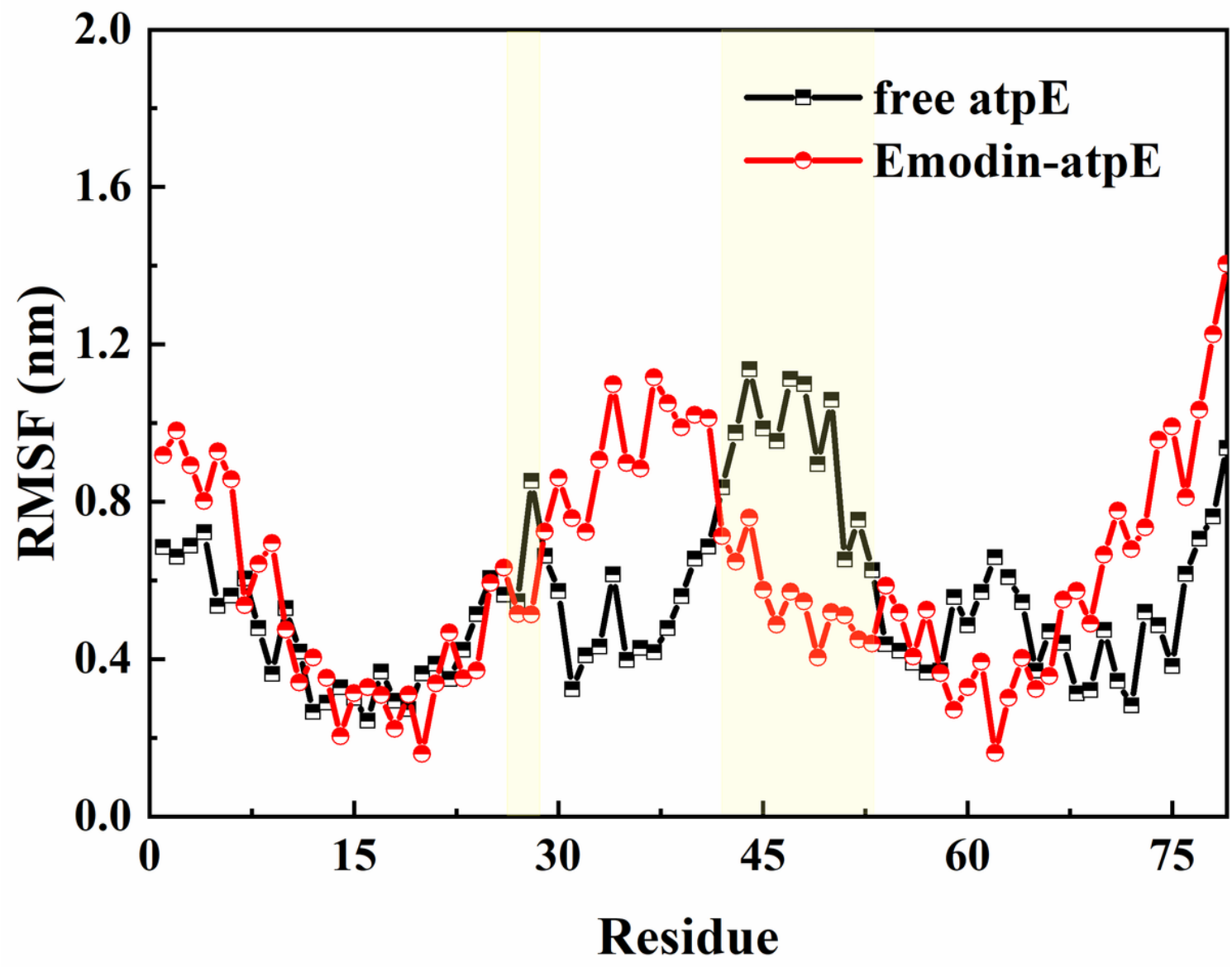

Figure 4

The RMSF of all residues (1-79) within the 10 ns simulation with regard to the initial positions of the atpE-emodin complex. The region of the protein backbone appeared to depend on local environment fluctuations (bound to emodin).

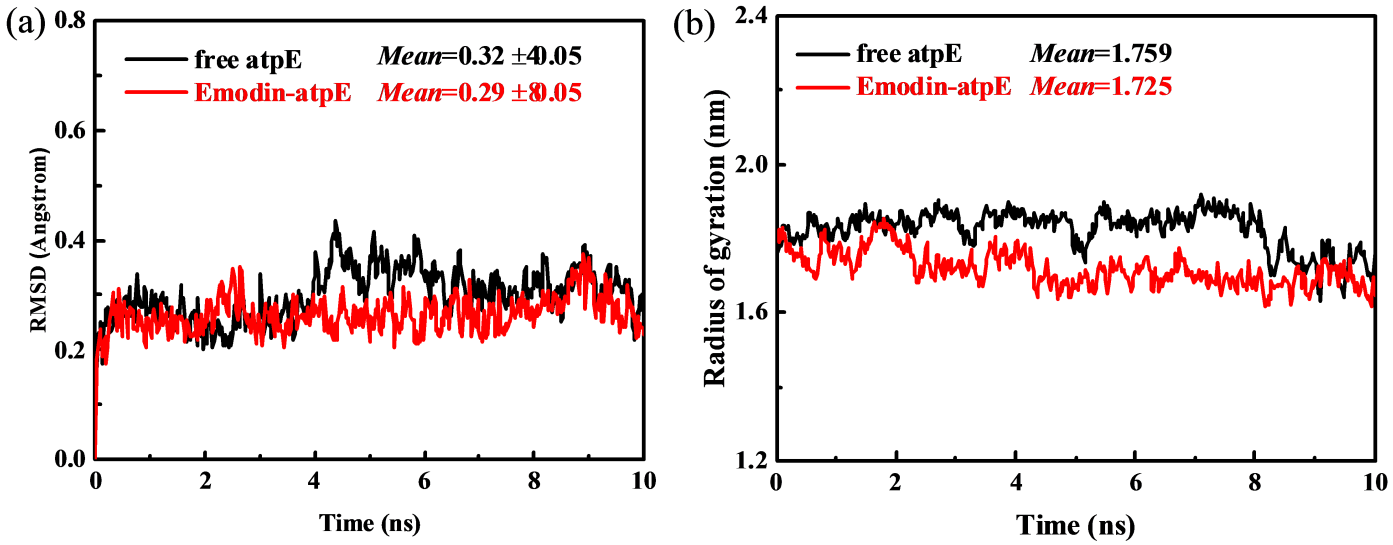

Figure 5

(a) The RMSD showed by the backbone atoms of free atpE and emodin-atpE during MD simulations was presented by using Gromacs 5.1.3 software. (b) The radius of gyration of atpE was a function of the simulation time.

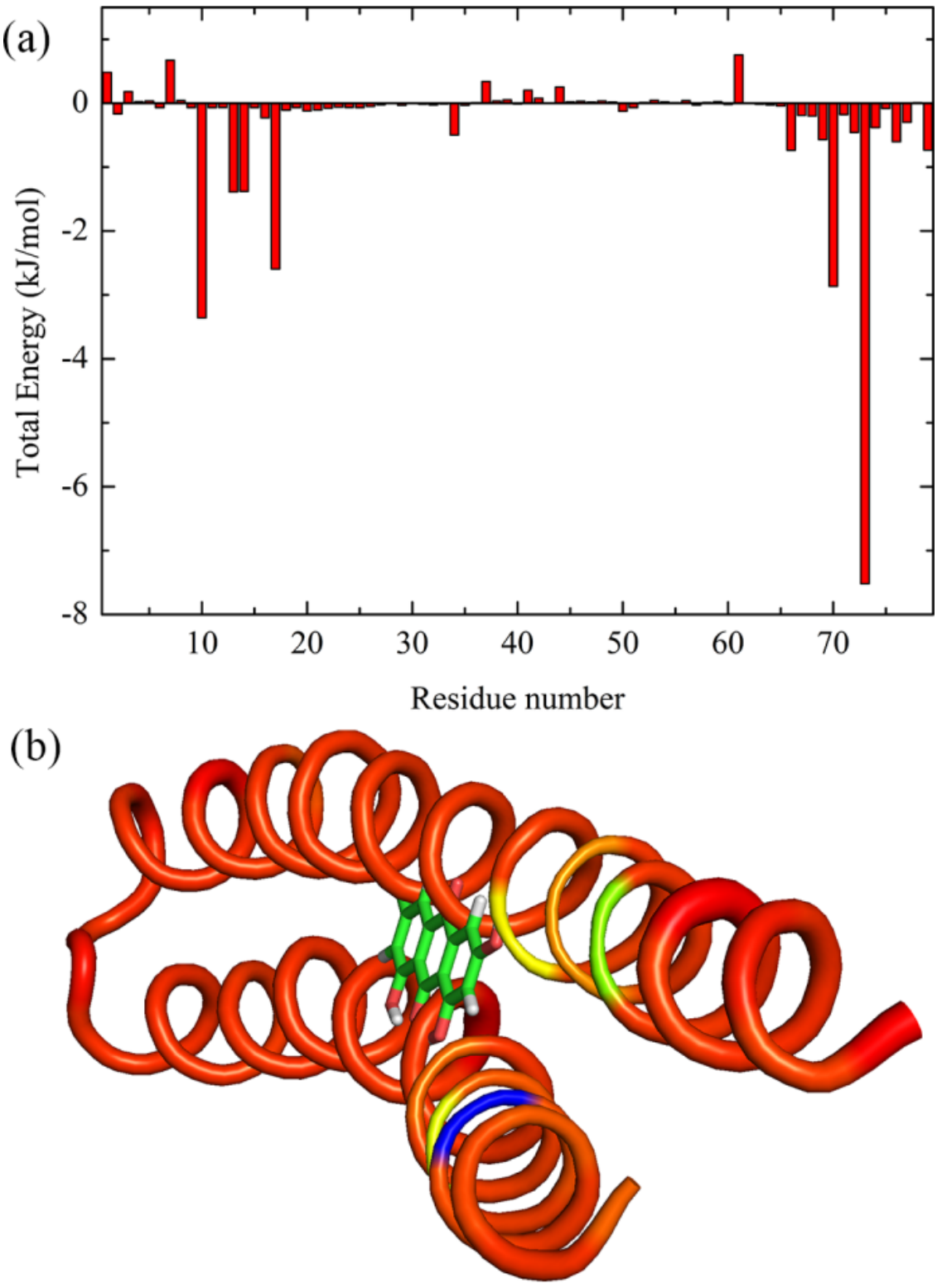

Figure 6

The residue-based energy decomposition on all residues. (a) The histogram chart showed the contributions of all the residues for the complexes. (b) The binding mode of emodin with atpE. In this binding mode, color from red to blue represented total free energy from low to high.

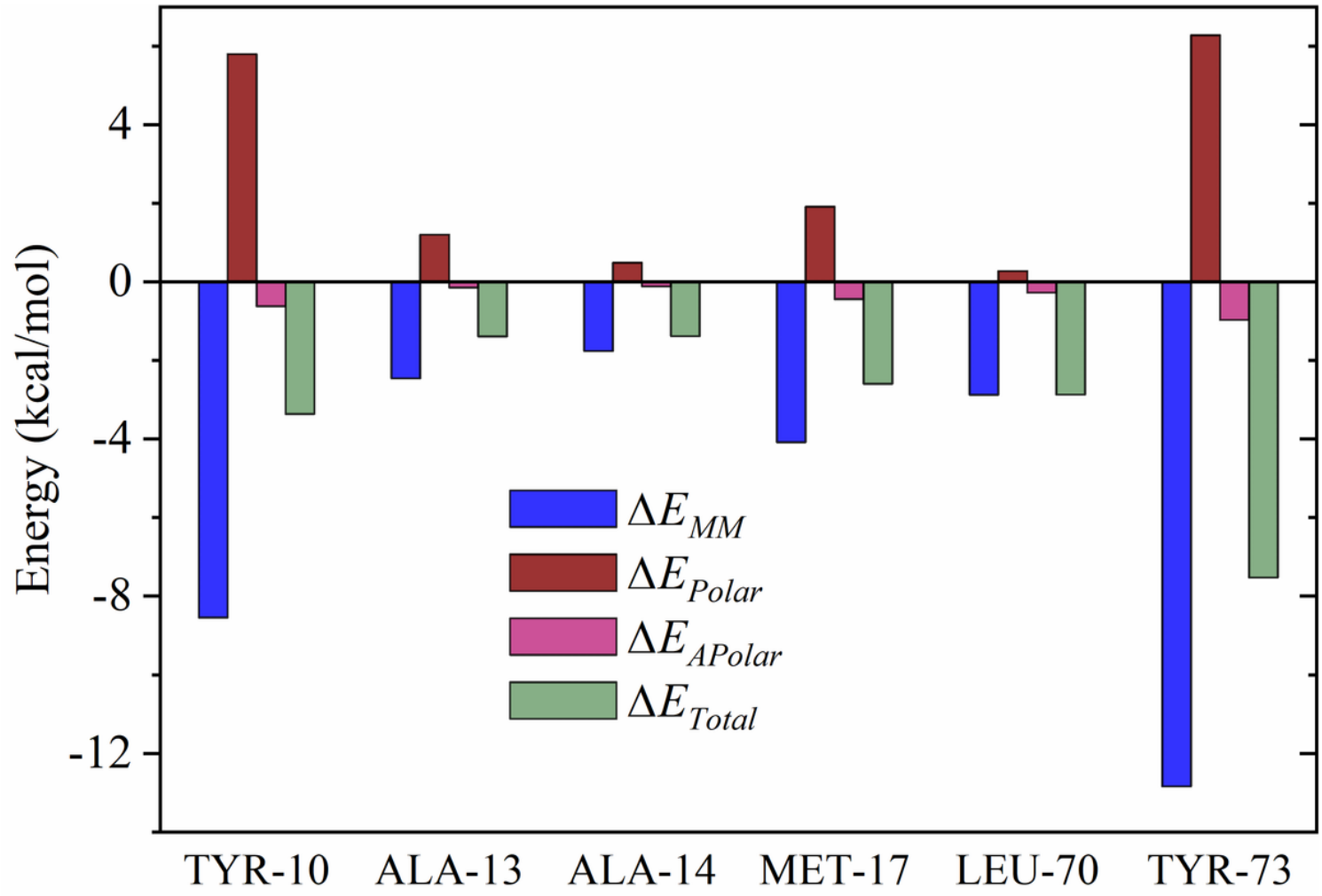

Figure 7

The residue-based energy decomposition of molecular mechanics, polar, nonpolar and total contributions on all residues

Supplementary Files

This is a list of supplementary files associated with this preprint. Click to download.

- Graphicalabstract.docx